



Contents lists available at ScienceDirect

Journal of the Mechanics and Physics of Solids

journal homepage: www.elsevier.com/locate/jmps

Regularized formulation of the variational brittle fracture with unilateral contact: Numerical experiments

Hanen Amor^a, Jean-Jacques Marigo^b, Corrado Maurini^{b,*}

^a LPMTM (CNRS-UPR 9001) and LAGA (CNRS-UMR 7539), Institut Galilée, Univ Paris-Nord, 99 avenue Jean-Baptiste Clément, 93430 Villetaneuse, France

^b Institut Jean Le Rond d'Alembert, UPMC Univ Paris 06 and CNRS (UMR 7190), 4 place Jussieu, 75252 Paris Cedex 05, France

ARTICLE INFO

Article history:

Received 10 January 2009

Received in revised form

23 April 2009

Accepted 24 April 2009

Keywords:

Fracture

Energy methods

Free-discontinuity problems

Contact mechanics

Finite elements

ABSTRACT

This paper presents a modified regularized formulation of the Ambrosio–Tortorelli type to introduce the crack non-interpenetration condition in the variational approach to fracture mechanics proposed by Francfort and Marigo [1998. Revisiting brittle fracture as an energy minimization problem. *J. Mech. Phys. Solids* 46 (8), 1319–1342]. We focus on the linear elastic case where the contact condition appears as a local unilateral constraint on the displacement jump at the crack surfaces. The regularized model is obtained by splitting the strain energy in a spherical and a deviatoric parts and accounting for the sign of the local volume change. The numerical implementation is based on a standard finite element discretization and on the adaptation of an alternate minimization algorithm used in previous works. The new regularization avoids crack interpenetration and predicts asymmetric results in traction and in compression. Even though we do not exhibit any gamma-convergence proof toward the desired limit behavior, we illustrate through several numerical case studies the pertinence of the new model in comparison to other approaches.

© 2009 Elsevier Ltd. All rights reserved.

1. Introduction

Computational approaches for simulating fracture of solids at the macroscopic scale are commonly classified into two categories (see e.g. de Borst et al., 2004): (i) discrete crack models with an explicit geometric modeling of cracks as surfaces of discontinuities and (ii) smeared crack models, approximating cracks with continuum fields having high gradients localized in thin bands.

The implementation of discrete crack approaches requires specific techniques to introduce discontinuous fields in the numerical model. The classical method consists in changing the mesh geometry by introducing new boundaries as the crack propagates together with adaptive remeshing (Ingraffea and Saouma, 1984). Efficient alternatives are the extended finite element methods (Moës et al., 1999), which enrich the finite element shape functions with discontinuous fields on the basis of a partition of unity concept (Babuska and Melenk, 1997), and interelement crack methods (Xu and Needleman, 1994; Camacho and Ortiz, 1996), which constrain cracks to propagate along the element interfaces.

Smeared crack (or continuum) approaches, include *damage models* (see e.g. Jirasek, 1998; Pijaudier-Cabot and Bazant, 1987; Lorentz and Andrieux, 1999) and *diffuse interface* (or *phase-field*) models (Aranson et al., 2000; Hakim and Karma, 2009; Marconi and Jagla, 2005). In the comparative study of Song et al. (2008), these approaches are synthetically classified as *element deletion methods*. They are based on the use of phenomenological constitutive laws with strain-softening. It is

* Corresponding author. Tel.: +33 1 44 27 87 19; fax: +33 1 44 27 52 59.

E-mail address: corrado.maurini@upmc.fr (C. Maurini).

well known that they require to account for some kind of non-local effects and the introduction of an internal length to penalize extreme strain localization and avoid the bad-posedness of the boundary value problem.

The use of each of the computational methods calls for suitable crack (or damage) propagation laws. Remarkable results have been obtained coupling the discrete crack approach with cohesive force models (Xu and Needleman, 1994; Camacho and Ortiz, 1996; Ortiz and Pandolfi, 1999; Moës and Belytschko, 2002; Meschke and Dumstorff, 2007; Remmers et al., 2008), and the smeared crack approach with non-local damage models of integral (see e.g. Jirasek, 1998) or gradient (see e.g. Peerlings et al., 1998; Lorentz and Benallal, 2005) type. However, fundamental questions on the quality of the numerical approximation concern the dependence of the results on the finite element meshes and the convergence of the solutions when the mesh size and/or the internal lengths eventually introduced in the model tend to zero. Even though several works attempt to establish an equivalence between the discrete and the smeared approaches (Mazars and Pijaudier-Cabot, 1996; Oliver et al., 2002; Mariani and Perego, 2003; de Borst et al., 2004; Cazes et al., 2009), the link between damage and fracture remains vague in most of the literature. This point becomes even more hazy when considering the introduction of the unilateral contact constraint at the crack interfaces (see e.g. Ramtani et al., 1992; Comi, 2001).

In this panorama, the variational approach to fracture proposed by Francfort and Marigo (1998) has the merit to open the path for a mathematically deep-rooted theory. It associates a clearly defined and general criterion for crack propagation with a consistent numerical solution strategy (Bourdin et al., 2000) able to account for complex fracture phenomena in space (multifissuration, crack branching and coalescence) and time (initiation, brutal propagation). The criterion for quasi-static crack propagation consists in the minimization of an energy functional defined as the sum of a bulk term, the elastic energy of the cracked body, and a surface term, the crack energy. The minimization has to be taken among all the possible cracks sets, which must respect an irreversibility condition to avoid unphysical self-healing. The variational problem finds its proper mathematical setting in the modern theory of the calculus of variations, where it is classified as a *free-discontinuity problem* to be studied in the framework of spaces of *special functions of bounded variations* (SBV) and their variants (Ambrosio et al., 2000). Existence of solutions and convergence of time-discrete formulations toward consistent time-continuous quasi-static evolutions is proved by Dal Maso and Toader (2002) for 2-D antiplane shear, by Francfort and Larsen (2003) for the n -dimensional case including cracks with an arbitrary number of connected components, and by Chambolle (2003, 2004) for plane elasticity with vectorial displacement fields. The effect of considering surface energies of the Griffith or cohesive type is discussed in Bourdin et al. (2008).

The mathematical theory of free-discontinuity problems provides several effective tools to obtain approximate solutions of the variational problem of fracture mechanics. The most adopted strategy is due to Ambrosio and Tortorelli (1990). Being initially developed for image segmentation applications (Mumford and Shah, 1989), it is adapted to the fracture problem in Bourdin et al. (2000) and Bourdin (2007). It is based on the approximation of the original energy functional with a regularized elliptic functional introducing an auxiliary scalar field and a small parameter. When the small parameter tends to zero, the elliptic functional convergences, in the sense of gamma-convergence, to the original one. Minimizers of the new functional are characterized by bands having a thickness of the order of the small parameter, where the gradients of the displacement field concentrate. These bands are a regularized representation of the cracks. Remarkably, the regularized model may be regarded as a damage model of the gradient type (Liebe et al., 2001; Lorentz and Benallal, 2005; Benallal and Marigo, 2007), the auxiliary field being the damage field, the small parameter the associated internal length. The gamma-convergence result proves that when the internal length tends to zero, gradient damage models with specific constitutive properties converge toward a model of brittle fracture of the Griffith type (Brides, 1998; Chambolle, 2004; Giacomini, 2005). In this sense, the mathematical theory of free-discontinuity problems and gamma-convergence theorems give a precise sense to the intuitive idea of using smeared crack approaches to approximate brittle fracture with discrete cracks (Brides, 1998; Lussardi and Negri, 2007). The availability of several rigorous results about the convergence of finite element discretizations (Bellettini and Coscia, 1994) and the influence of the meshes on the crack propagation conditions (Negri, 1999) makes the variational approach a reliable tool for the numerical simulation of fracture phenomena.

This paper discusses a regularized model to introduce the unilateral contact condition in the variational approach of fracture mechanics. Unilateral contact at the crack lips is not considered in the initial works on the subject. The regularized model adopted in Bourdin et al. (2000, 2008) is characterized by a symmetric behavior in traction and in compression and allows for negative displacement jumps, i.e. material interpenetration in cracks associated to compressive actions. Numerical approaches avoiding material interpenetration are proposed by Lancioni and Royer-Carfagni (2009) and Del Piero et al. (2007). Lancioni and Royer-Carfagni introduce a regularized variational model permitting only shear damage, approximation of mode-II cracks. Their model keeps a symmetric behavior in traction and compression. It rules out material interpenetration by completely forbidding crack openings. It is suitable for compressed materials, but it appears unrealistic in expanded regions, where open fractures are expected. Del Piero et al. (2007), considering the extension of the variational approach in the context of non-linear elasticity, formulate a model avoiding material interpenetration in compression by penalizing extreme volume deformations using an elastic energy density function of the Ogden type. Hence, they apply the Ambrosio–Tortorelli regularization strategy to numerically solve the variational problem with standard finite element techniques. The numerical results clearly show the desired non-symmetric behavior for traction and compression tests. However, material failure in compression displays diffuse damage without a distinct convergence toward sharp cracks. The resulting rupture mechanism remains difficult to be interpreted both from the physical and the mathematical point of view. Giacomini and Ponsiglione (2008) studied the mathematical properties of the variational

problem including frictionless self-contact without interpenetration of matter. Considering a geometrically non-linear model where the non-interpenetration condition appears as a non-local injectivity constraint and polyconvex elastic energies density of the Ogden type, they concluded with an existence result. However, in the apparently simpler framework of linearized elasticity, where the unilateral contact condition appears as a local unilateral constraint on the admissible displacement jumps, mathematical results are not available at the moment, neither about the existence of solutions, nor about convergent regularized formulations à la Ambrosio–Tortorelli.

Here we present a regularized model of the Ambrosio–Tortorelli type that introduces the effect of unilateral contact and accounts for asymmetric behaviors in traction and compression in the framework of linearized elasticity. The new regularized formulation is inspired by the mechanical interpretation of the standard Ambrosio–Tortorelli approximation as a non-local damage model. Sharing the spirit of works introducing unilateral effects in isotropic damage models (Ramtani et al., 1992; Comi, 2001), it is based on the splitting of the strain energy in a spherical and a deviatoric parts and on the introduction an energy density depending on the sign of the local volume change. Its numerical implementation adopts a standard finite element technique and an alternate minimization algorithm.

The exposition starts recalling the variational formulation of fracture mechanics (Section 2). We distinguish among models not accounting for contact conditions, models where only shear fractures are allowed, and models introducing unilateral contact effects. Section 3, considering the basic example of uniaxial compression, shows that the model with shear fracture and the model with unilateral contact put forth existence issues for the variational problem. In Section 4, we propose a modification of the standard Ambrosio–Tortorelli regularized formulation to account for unilateral effects. Although we will not provide any rigorous proof of the convergence toward the desired limit behavior, the effectualness of the proposed regularized model is corroborated by the numerical results. To this end, after providing some details on the numerical implementation (Section 5), we revisit two numerical case studies considered in previous works (Section 6). The comparison of several models assesses the effect of the contact conditions on the crack patterns.

2. Brittle fracture as a free-discontinuity problem

2.1. Griffith energy functional

Consider a body $\Omega \subset \mathbb{R}^n$ with displacement U imposed on a part of its boundary, say $\partial_u \Omega$. Let Γ be the set of cracked points of the body, where the displacement field u may be discontinuous. The variational approach to fracture mechanics proposed by Francfort and Marigo (1998) introduces the following energy functional for the cracked body:

$$E(u, \Gamma) = E_d(u, \Gamma) + E_s(\Gamma) = \int_{\Omega \setminus \Gamma} W(\varepsilon(u)) \, dx + G_c \mathcal{H}^{n-1}(\Gamma), \quad (1)$$

where W is the elastic energy density, function of the linearized strain $\varepsilon(u)$, symmetric part of the gradient of u ; G_c is the fracture toughness (energy required to create a unit surface crack), and \mathcal{H}^{n-1} the Hausdorff surface measure giving the crack length ($n = 2$) or surface ($n = 3$). The bulk term of (1), $E_d(u, \Gamma)$, is the elastic energy stored in the cracked body; the surface term, $E_s(\Gamma)$, is the energy required to create the crack according to the Griffith model. For linear elastic bodies $W(\varepsilon) = 1/2 A \varepsilon \cdot \varepsilon$, where A is the fourth order elastic stiffness tensor. In the following, we will focus on the isotropic case for which, given the Lamé coefficients λ and μ , the elastic energy reads as

$$W(\varepsilon) = \frac{1}{2} \lambda \operatorname{tr}(\varepsilon)^2 + \mu \varepsilon \cdot \varepsilon. \quad (2)$$

2.2. Variational formulation with no-contact condition

The Francfort–Marigo model formulates the quasi-static time evolution of the displacement field u and the crack set Γ as a minimization problem on (1). In view of the numerical applications, we focus here on the time-discrete case, with $N + 1$ time steps $\{t_0 = 0, \dots, t_i, \dots, t_N = T\}$ and displacement loadings linearly increasing in time, say $U(t, x) = t\bar{U}(x)$. On the basis of the knowledge of the state at the time instant t_{i-1} , the state at the time step t_i is obtained as the solution of the following minimization problem:

$$\inf \{E(u, \Gamma) : u \in \mathcal{C}(\Gamma, t_i), \Gamma \supseteq \Gamma_{i-1}\}, \quad (3)$$

where the space of admissible displacements at time t is

$$\mathcal{C}(\Gamma, t) := \{u \in H^1(\Omega \setminus \Gamma), u(x) = t\bar{U}(x) \text{ on } \partial_u \Omega\}, \quad (4)$$

while the admissible crack sets have to satisfy the *irreversibility condition* $\Gamma \supseteq \Gamma_{i-1}$. The latter condition is fundamental to prevent the healing of the crack set Γ_{i-1} at the previous time step. The problem (3) presents formidable difficulties because of the arbitrariness of the crack set Γ . Problems of this type, where the unknowns are a field (u) and its jump set (Γ), are referred as *free-discontinuity problems* (Ambrosio et al., 2000).

The formulation of Francfort and Marigo (1998) is based on *global* energy minimization at each time step. This formulation mends the well-known limits of the Griffith model on initiation, selection of the crack pattern, and brutal

propagation problems. Namely, for proportional loadings crack initiation always occurs in finite time, the selection of the crack pattern is a part of the minimization process without requiring any *a priori* assumption, and the crack propagation may be discontinuous in time whenever it turns out to be beneficial for energy minimization. As discussed in detail in Bourdin et al. (2008), the model precludes the possibility of force loadings because the associated global minimization problem is not well posed.

A fundamental limit of the formulation based on (3) and (4) is the absence of any contact condition at the crack lips in the space of admissible displacement $\mathcal{C}(\Gamma, t)$. The displacement jump across the crack may be arbitrary. The component normal to the crack surface may be either positive (crack opening) or negative (crack interpenetration). In particular, the functional (1) being a symmetric function of u and $\mathcal{C}(\Gamma, t)$ being an affine space, if $\{u_i, \Gamma_i\}_{i=1}^N$ is a solution for the loading $\bar{U}(x)$, then $\{-u_i, \Gamma_i\}_{i=1}^N$ is a solution for the opposite loading $-\bar{U}(x)$. Hence, any example leading to crack opening, as the uniaxial traction studied in Francfort and Marigo (1998), automatically implies an unphysical crack interpenetration for the opposite loading.

2.3. Variational formulation for shear fracture

A simple solution to avoid crack interpenetration in compression is to formulate a model where only shear mode fracture is permitted. In a variational formulation of the type (3), such a model is distinguished by an additional condition on the admissible displacements. Namely, the minimization problem (3) should be reformulated as

$$\inf\{E(u, \Gamma) : u \in \tilde{\mathcal{C}}(\Gamma, t_i), \Gamma \supseteq \Gamma_{i-1}\}, \quad (5)$$

where the space of admissible displacements is restricted to

$$\tilde{\mathcal{C}}(\Gamma, t) := \{u \in H^1(\Omega \setminus \Gamma), u(x) = t\bar{U}(x) \text{ on } \partial_u \Omega, \llbracket u \rrbracket \cdot n = 0 \text{ on } \Gamma\}. \quad (6)$$

The space $\tilde{\mathcal{C}}(\Gamma, t)$ admits only fields with a vanishing component of the displacement jump $\llbracket u \rrbracket$ along the normal n to the crack surface. As before, the space of admissible displacement is an affine space and the symmetry of $E(u, \Gamma)$ with respect to u implies that opposite loadings lead to solutions with opposite displacements and the same crack pattern.

2.4. Variational formulation with unilateral contact

A more realistic model of brittle fracture should allow for crack opening, but prevent crack interpenetration by including an unilateral contact condition at the crack lips. Such a model corresponds to the variational formulation

$$\inf\{E(u, \Gamma) : u \in \hat{\mathcal{C}}(\Gamma, t_i), \Gamma \supseteq \Gamma_{i-1}\}, \quad (7)$$

where the minimization is taken over the restricted space of admissible displacements

$$\hat{\mathcal{C}}(\Gamma, t) := \{u \in H^1(\Omega \setminus \Gamma), u(x) = t\bar{U}(x) \text{ on } \partial_u \Omega, \llbracket u \rrbracket \cdot n \geq 0 \text{ on } \Gamma\}. \quad (8)$$

The space $\hat{\mathcal{C}}(\Gamma, t)$ includes only the displacement fields with a non-negative normal component of the displacement jump at the crack lips. It is not any more an affine space, but a convex cone. Because of the unilateral contact condition, opposite loadings may lead to completely different solutions. It is interesting to note that since

$$\tilde{\mathcal{C}}(\Gamma, t) \subseteq \hat{\mathcal{C}}(\Gamma, t) \subseteq \mathcal{C}(\Gamma, t), \quad (9)$$

then

$$\inf_{u \in \hat{\mathcal{C}}(\Gamma, t_i)} E_d(u, \Gamma) \leq \inf_{u \in \tilde{\mathcal{C}}(\Gamma, t_i)} E_d(u, \Gamma) \leq \inf_{u \in \mathcal{C}(\Gamma, t_i)} E_d(u, \Gamma), \quad (10)$$

i.e. the strain energy for a given crack set in the case of shear fracture is larger than the energy of the model with unilateral contact, which in turns is larger than the energy of the model with no-contact.

The above model for unilateral contact neglects friction effects. Including them in the variational model would demand the introduction of additional state variables and energy contributions (see e.g. Raous et al., 1999). This important issue remains out of the scope of the present paper.

3. Existence issues

Direct methods of the calculus of variations provide existence results for the minimization problem (3) by resorting to a *weak* formulation based on the introduction of spaces of special functions with bounded variations which allows for the discontinuity of the displacement field on an unknown set of jump points (Ambrosio et al., 2000). Proofs of existence of solutions and convergence of the time-discrete quasi-static evolution are available for antiplane linear elasticity (Dal Maso and Toader, 2002; Francfort and Larsen, 2003) and for general linear (Chambolle, 2003) and non-linear (Dal Maso et al., 2005) elasticity without contact conditions. Giacomini and Ponsiglione (2008) discuss the case of the unilateral contact problem in the geometrically non-linear framework where the non-interpenetration condition translates into an injectivity

constraint. No existence theorems are available for the geometrically linearized shear fracture model and the unilateral contact model, where the minimization problem is restricted over the spaces of admissible displacements (6) and (8), respectively. Analyzing the simple example of uniaxial compression of a cylinder, we show below that existence is really an issue in those cases.

3.1. Uniaxial compression of a 3-D cylinder: a case of non-existence of solutions

Francfort and Marigo (1998) illustrated analytically the solution of the minimization problem (3) for the uniaxial traction of a 3-D cylinder within the model with no-contact condition. Here we revisit this problem for compressive loading with the model accounting for the unilateral contact at the crack lips.

We consider an initially crack-free cylinder $\Omega \equiv S \times (0, L)$, S being a smooth bounded open connected domain of \mathbb{R}^2 , made of an isotropic and homogeneous material with Young’s modulus Y , Poisson’s ratio ν , and fracture toughness G_c . The components u_i of a vector u will be referred to an orthogonal reference system $\{0, e_1, e_2, e_3\}$ with the e_3 -axis oriented along the axis of the cylinder (see Fig. 1a). The boundary conditions impose a null axial displacement at $x_3 = 0$ and an axial displacement t at $x_3 = L$. The other components of the displacements are free, the cylinder bases being free to slide without friction on the support. The cylinder mantle is free. Hence, for the model with no-contact condition considered in Francfort and Marigo (1998), the space of admissible displacements is

$$\mathcal{C}(\Gamma, t) \equiv \{v \in H^1(\Omega \setminus \Gamma; \mathbb{R}^2), v_3 = 0 \text{ on } S \times 0, v_3 = t \text{ on } S \times L\}. \tag{11}$$

For the model with unilateral contact admissible displacements must be in

$$\widehat{\mathcal{C}}(\Gamma, t) \equiv \{v \in \mathcal{C}(\Gamma, t), \llbracket u \rrbracket \cdot n \geq 0 \text{ on } \Gamma\}. \tag{12}$$

In the two cases, we introduce the following notation for the elastic energy and the total energy for a given crack state Γ and loading parameter t :

$$E_d^{(t)}(\Gamma) = \inf_{u \in \mathcal{C}(\Gamma, t)} E_d(u, \Gamma), \quad E^{(t)}(\Gamma) = E_d^{(t)}(\Gamma) + E_s(\Gamma), \tag{13}$$

$$\widehat{E}_d^{(t)}(\Gamma) = \inf_{u \in \widehat{\mathcal{C}}(\Gamma, t)} E_d(u, \Gamma), \quad \widehat{E}^{(t)}(\Gamma) = \widehat{E}_d^{(t)}(\Gamma) + E_s(\Gamma). \tag{14}$$

For the initial uncracked state $\Gamma_0 = \emptyset$, $E_s(\emptyset) = 0$ and the total energy is given by

$$E^{(t)}(\emptyset) = \widehat{E}^{(t)}(\emptyset) = \frac{1Y|S|}{2L} t^2, \tag{15}$$

where $|S|$ is the cross sectional area. For a generic crack set Γ , denoting by $P(\Gamma)$ the projection of the crack set onto the cross-section S and by $\Theta(\Gamma) = \mathcal{H}^2(P(\Gamma))/|S|$ the damaged ratio of cross sectional area, the following estimate from below of the total energy of the model with no-contact conditions holds (see Francfort and Marigo, 1998, Proposition 3.1):

$$E^{(t)}(\Gamma) \geq (1 - \Theta(\Gamma))E(\emptyset, t) + G_c\Theta(\Gamma)|S|. \tag{16}$$

Noting that $\widehat{E}^{(t)}(\Gamma) \geq E^{(t)}(\Gamma)$ and $\widehat{E}^{(t)}(\emptyset) = E^{(t)}(\emptyset)$, the analog estimate holds true also for the model with unilateral contact, i.e.:

$$\widehat{E}^{(t)}(\Gamma) \geq (1 - \Theta(\Gamma))\widehat{E}(\emptyset, t) + G_c\Theta(\Gamma)|S|. \tag{17}$$

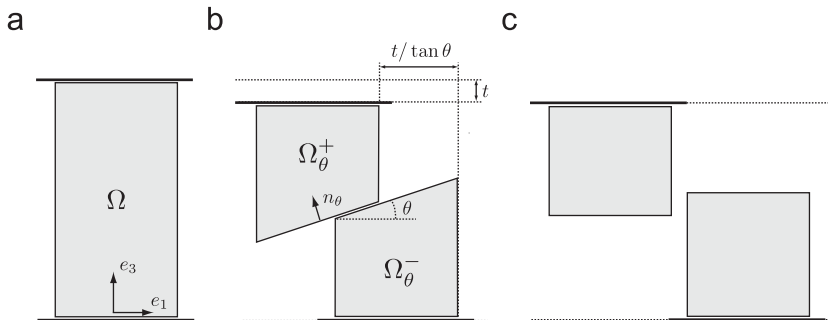


Fig. 1. Uniaxial compression as an example of non-existence of solutions for the linearized unilateral contact model: (a) reference configuration; (b) linearized model: a plane crack minimizing sequence with rigid-body displacements which does not converge for $\theta \rightarrow 0$; (c) geometric non-linear model: the solution with rigid-body displacements.

Moreover, we may prove an estimate from above of the infimum of the energy:

Proposition 3.1. For all loadings $t \in \mathbb{R}$,

$$\inf_{\Gamma} \widehat{E}^{(t)}(\Gamma) = \inf_{\Gamma} \inf_{u \in \mathcal{C}(\Gamma, t)} \widehat{E}(u, \Gamma) \leq G_c |S|. \quad (18)$$

Proof. The case $t \geq 0$ is trivial. For $t < 0$, consider the following family of admissible pairs of crack sets and displacement fields $(\Gamma_\theta, u_\theta \in \widehat{\mathcal{C}}(\Gamma_\theta, t))$ with $0 < \theta < \theta_{max}$ corresponding to a plane crack of normal $n_\theta = -\sin \theta e_1 + \cos \theta e_3$ passing through a point $\bar{x} \in \Omega$ and cutting the cylinder into two rigid parts $\Omega_\theta^+ \equiv \{x \in \Omega, (x - \bar{x}) \cdot n_\theta > 0\}$ and $\Omega_\theta^- \equiv \{x \in \Omega, (x - \bar{x}) \cdot n_\theta < 0\}$ without intersecting the bases $x_3 = 0, L$ (see Fig. 1b):

$$\Gamma_\theta \equiv \{x \in \Omega : (x - \bar{x}) \cdot n_\theta = 0\}, \quad (19)$$

$$u_\theta = \begin{cases} u_\theta^+ = t(1/\tan \theta e_1 + e_3), & x \in \Omega_\theta^+, \\ u_\theta^- = 0, & x \in \Omega_\theta^-. \end{cases} \quad (20)$$

The associated strain energy is null and the total energy is $\widehat{E}(u_\theta, \Gamma_\theta) = G_c |S| / \cos \theta$. Hence, $(\Gamma_\theta, u_\theta)$ with θ sufficiently small (but positive) is an admissible pair whose energy approaches arbitrarily close to the value $G_c |S|$. \square

Using the estimates (17) and (18), we derive the following results about the solution of the minimization problem (7) of the model with unilateral contact:

Proposition 3.2. For traction loadings ($t \geq 0$), the cylinder remains crack free as long as

$$0 \leq t < t_r = \sqrt{2(kL/Y)}.$$

For $t > t_r$ a solution-crack consists in cutting the cylinder into two pieces along an arbitrary transverse section.

Proof. The proof in Francfort and Marigo (1998) for the model with no-contact can be repeated without modifications. We recall here only the reasoning for $t > t_r$, which is fundamental for the next proposition. Since $\widehat{E}_d^{(t)}(\emptyset) > G_c |S|$, the estimate (17) implies that $\widehat{E}^{(t)}(\Gamma) \geq G_c |S|$. Moreover, $\widehat{E}^{(t)}(\Gamma) = G_c |S|$ only if $\Theta(\Gamma) = 1$, i.e. $P(\Gamma) = S$, $\mathcal{H}^2(\Gamma) = |S|$ and $\widehat{E}_d^{(t)}(\Gamma) = 0$. Hence, the optimal displacement field must be a piecewise rigid displacement, respecting the boundary conditions $u_3 = 0$ on $x_3 = 0$ and $u_3 = t$ on $x_3 = L$. The only cracked state respecting the conditions above is a transverse crack $\Gamma \equiv S \times \bar{z}$ with $\bar{z} \in [0, L]$ dividing the solid into two connected domains $\Omega_\theta^+ \equiv \{x \in \Omega, z > \bar{z}\}$ and $\Omega_\theta^- \equiv \{x \in \Omega, z < \bar{z}\}$ experiencing rigid displacements of the form

$$u = \begin{cases} u^- = a_1 e_1 + a_2 e_2, & x \in \Omega_\theta^-, \\ u^+ = b_1 e_1 + b_2 e_2 + t e_3, & x \in \Omega_\theta^+, \end{cases} \quad (21)$$

where a_1, a_2, b_1, b_2 are arbitrary constants. This concludes the proof for the model with no-contact. In the unilateral contact case, we must additionally check that the crack jump on Γ is admissible, i.e. that $[[u]] \cdot n \geq 0$ on Γ . This condition is verified for the traction loadings because

$$[[u]] \cdot n = (u^+ - u^-) \cdot e_3 = t > 0. \quad \square$$

Proposition 3.3. For compression loadings ($t \leq 0$), the cylinder remains crack free as long as

$$0 \geq t > -t_r = -\sqrt{2(kL/Y)}.$$

For $t < -t_r$ the minimization problem (7) for the unilateral contact model does not admit a solution.

Proof. We prove only the part for $t < -t_r$. The estimate (17) implies that with $t < -t_r$, $\widehat{E}^{(t)}(\Gamma) \geq G_c |S|$. Hence, in view of (18) the minimum value of $\widehat{E}^{(t)}(\Gamma)$, if it exists, should be exactly equal to $G_c |S|$. Repeating the reasoning of the previous proposition one can show that, for $t < -t_r$, the only class of crack states and displacement fields respecting the boundary conditions in $x_3 = 0$ and $x_3 = L$ for which $\widehat{E}^{(t)}(\Gamma) = G_c |S|$ is a transverse crack cutting the solids into two parts with rigid displacements in the form (21). But in this case

$$[[u]] \cdot n = (u^+ - u^-) \cdot e_3 = t < 0$$

and the states attaining the limit value of the energy (18) are not compatible with the unilateral contact condition. We conclude that for $t < -t_r$ the minimization problem of the model with unilateral contact does not admit a solution. \square

Remarks.

- For the shear fracture model characterized by the admissible displacements (6) the same result as in Proposition 3.3 holds for both traction ($t > 0$) and compression ($t < 0$) loadings. The shear fracture model presents existence issues in both cases. In particular, the analogs of estimates (17) and (18) stay true because $\tilde{\mathcal{U}}(\Gamma, t) \subseteq \mathcal{U}(\Gamma, t)$.
- Our construction of a minimizing sequence to prove non-existence of a minimum fails if we change the boundary conditions at the bases of the cylinder. However, that does not mean that existence is recovered if we control the tangential displacements at the bases.
- In the proposed counterexample, the minimization problem does not admit a solution because the minimizing sequence (19)–(20) does not converge for $\theta \rightarrow 0$. Possible artificial remedies to recover the existence of solution include the introduction of a upper bound on the norm of allowable displacements or of a residual stiffness in the cracked surface. As a drawback, the solution will depend on the associated non-physical constants.
- Differently from the existence issues encountered for force loadings (see Bourdin et al., 2008), here the problems come from the linearized kinematics. In the geometric non-linear framework, where the non-interpenetration condition reads as injectivity constraint on the displacement map (see e.g. Ciarlet and Nečas, 1987), the minimization problem enjoys existence of solutions, as proved by Giacomini and Ponsiglione (2008). In the case of the uniaxial compression considered here, a possible solution for $t < -t_r$ is obtained by cutting the cylinder into two rigid parts with a plane parallel to the bases. Interpenetration is avoided by translating one of the two parts along e_1 , as sketched in Fig. 1c.

4. Regularized models: approximation by elliptic functionals

The minimization problem for the quasi-static crack evolution as formulated in (3) is not prone to an immediate numerical implementation. To tackle it numerically with a standard finite element discretization, Bourdin et al. (2000) resort to a regularization strategy proposed by Ambrosio and Tortorelli (1990) for solving similar free-discontinuity problems encountered in image segmentation (Mumford and Shah, 1989). Lancioni and Royer-Carfagni (2009) propose a variant of the regularized formulation to reproduce the behavior of the shear fracture model. Here, after recalling these approaches, we present a tentative regularized variational formulation for the model including unilateral contact effects. At present time, rigorous gamma-convergence results are available only for the model with no-contact condition.

4.1. Regularized model with no-contact condition

To approximate the solution of the minimization problem (3) for the no-contact model, Bourdin et al. (2000) adopted the following one-parameter family of elliptic functionals:

$$\mathcal{E}_\ell(u, \alpha) = \mathcal{P}(u, \alpha) + G_c \mathcal{S}_\ell(\alpha), \tag{22}$$

with

$$\mathcal{P}(u, \alpha) = \int_\Omega \frac{1}{2} (a(\alpha) + k_\ell) A \varepsilon(u) \cdot \varepsilon(u) \, dx, \tag{23}$$

$$\mathcal{S}_\ell(\alpha) = \int_\Omega \left(\frac{w(\alpha)}{\ell} + \ell \nabla \alpha \cdot \nabla \alpha \right) \, dx, \tag{24}$$

where ℓ and k_ℓ are positive scalar parameter, α is an additional scalar field¹ with values in $[0, 1]$, and

$$a(\alpha) = (1 - \alpha)^2, \quad w(\alpha) = \alpha^2/4. \tag{25}$$

The associated regularized version of the minimality principle (3) for the time-discrete quasi-static evolution between the time steps t_{i-1} and t_i reads as

$$\inf \{ \mathcal{E}_\ell(u, \alpha) : u \in \mathcal{U}^{(i)}, \alpha \in \mathcal{A}^{(i)} \}, \tag{26}$$

where the spaces of admissible state fields at the step i are

$$\mathcal{U}^{(i)} := \{ u \in H^1(\Omega), u(x) = t_i \bar{U}(x) \text{ on } \partial_u \Omega \}, \tag{27}$$

$$\mathcal{A}^{(i)} := \{ \alpha \in H^1(\Omega), \alpha_{i-1} \leq \alpha \leq 1 \}. \tag{28}$$

The condition $\alpha \geq \alpha_{i-1}$ in the definition of the space $\mathcal{A}^{(i)}$ is the regularized version of the irreversibility condition $\Gamma \supseteq \Gamma_{i-1}$ in (3).

¹ In Ambrosio and Tortorelli (1990) and Bourdin et al. (2000) the additional field is denoted by v , with $v = 1 - \alpha$.

Gamma-convergence theorems (Braides, 1998; Chambolle, 2004) prove that, for $\ell \rightarrow 0^+$, the sequence $(\bar{u}_\ell, \bar{\alpha}_\ell)$, obtained as the *global* minimum of (22) for fixed ℓ , converges, in a specific weak sense, to the *global* minimum of (1). Moreover, Giacomini (2005) proves that the time-discrete quasi-discrete evolution obtained by minimizing the regularized functional under the irreversibility condition on α converges to the quasi-static evolution of the brittle fracture model of Francfort and Marigo (1998). Roughly speaking, convergence of $(\bar{u}_\ell, \bar{\alpha}_\ell)$, minimizer of the functional (22), toward $(\bar{u}, \bar{\Gamma})$, minimizer of the Griffith functional (1), means that the field $\bar{\alpha}_\ell$ localizes in thin bands where the gradient of \bar{u}_ℓ is high; these bands stand for the crack set $\bar{\Gamma}$ where \bar{u} is discontinuous. Moreover, on this kind of solutions $\mathcal{P}(u, \alpha)$ provides an approximation of the elastic energy of the cracked body, whilst $\mathcal{S}_\ell(\alpha)$ approximates the crack surface. The parameter k_ℓ is a residual stiffness introduced to secure the positive definiteness of the elastic energy. Its value should be sufficiently small. Convergence toward brittle fracture requires k_ℓ going to zero faster than ℓ .

Global minimization is at the basis of all the available mathematical results. Moreover, in the absence of strong singularities in the stress field, it is essential to reproduce initiation and brutal phenomena within the Griffith model associated with the energy functional (1) (see Bourdin et al., 2008). In numerical works, global minimization is not practicable. One may try, at best, to look for the *local* minima around the solution at the previous time step (Bourdin et al., 2000; Del Piero et al., 2007; Lancioni and Royer-Carfagni, 2009).

A formulation based on local minimization of the regularized functional may be mechanically interpreted as the quasi-static evolution of a gradient damage model as per Benallal and Marigo (2007). In this context ℓ is an additional material parameter, the internal length, the scalar field α represents the damage field, and $a(\alpha)A$ is the damaged elastic stiffness, where $\alpha = 0$ means a sound material, $\alpha = 1$ a completely damaged one. The function $w(\alpha)$ stays for the energy dissipated in a homogeneous damage process. Differently from the Griffith energy (1), the regularized functional recovers initiation and brutal phenomena in the absence of strong singularities also with local minimization. The internal length ℓ will determine the corresponding threshold values of the loading parameter.

4.2. Regularized model for shear fracture

Lancioni and Royer-Carfagni recently proposed a regularized formulation reproducing the behavior of the shear fracture model (Lancioni and Royer-Carfagni, 2009). On the basis of the mechanical interpretation of the regularized formulation as a damage model, they modified the Ambrosio–Tortorelli functional (22) to obtain a gradient damage model developing shear bands with localized damage approximating mode-II cracks. The approach is based on the orthogonal decomposition of the linearized strain tensor in its spherical and deviatoric components:

$$\varepsilon = \varepsilon_S + \varepsilon_D, \quad \varepsilon_S = \frac{1}{n} \text{tr}(\varepsilon)I, \quad \varepsilon_D = \varepsilon - \frac{1}{n} \text{tr}(\varepsilon)I, \quad (29)$$

where I denotes the n -dimensional identity tensor. With this decomposition, the strain energy density of a linear elastic isotropic material may be written as the sum of the spherical and deviatoric contributions:

$$W(\varepsilon) = \frac{1}{2} \lambda \text{tr}(\varepsilon)^2 + \mu \varepsilon : \varepsilon = \kappa_0 \frac{\text{tr}(\varepsilon)^2}{2} + \mu \varepsilon_D : \varepsilon_D, \quad (30)$$

where λ and μ are the Lamé coefficients and $\kappa_0 = \lambda + 2\mu/n$ is the bulk modulus of the material. The regularized formulation for shear fracture replaces the functional $\mathcal{E}_\ell(u, \alpha)$ of the variational statement (26) by

$$\tilde{\mathcal{E}}_\ell(u, \alpha) = \int_\Omega \tilde{W}(\varepsilon(u), \alpha) \, dx + G_c \mathcal{S}_\ell(\alpha) \quad (31)$$

with

$$\tilde{W}(\varepsilon, \alpha) = \left(\kappa_0 \frac{\text{tr}(\varepsilon)^2}{2} + (a(\alpha) + k_\ell) \mu \varepsilon_D : \varepsilon_D \right), \quad (32)$$

where the spherical part of the elastic energy density remains unaffected by the value of the scalar field α . The modified energy functional implies that the creation of additional surface energy may be compensated exclusively by a reduction of the deviatoric elastic energy.

4.3. Regularized model for fracture with unilateral contact condition at crack lips

A model with unilateral contact is expected to authorize crack opening in the regions where the material tends to expand and to forbid crack interpenetration in compressed regions. In the regularized setting, such a model should respond differently as a function of the sign of the volume change, i.e. the divergence of the displacement or, equivalently, the trace of the strain tensor. To implant a similar behavior in an energy minimization principle, it is useful to introduce the decomposition of the trace of the strain tensor in positive and negative parts: $\text{tr}^+(\varepsilon) = \max(\text{tr}(\varepsilon), 0)$ and $\text{tr}^-(\varepsilon) = \max(-\text{tr}(\varepsilon), 0)$, and further distinguish the contributions due to compression, expansion, and shear of the strain

energy, as follows:

$$W(\varepsilon) = \kappa_0 \frac{\text{tr}^-(\varepsilon)^2}{2} + \kappa_0 \frac{\text{tr}^+(\varepsilon)^2}{2} + \mu \varepsilon_D \cdot \varepsilon_D. \tag{33}$$

Our proposal for a regularized formulation of the model with unilateral contact is to substitute in the variational statement (26) the energy functional $\mathcal{E}_\ell(u, \alpha)$ with

$$\widehat{\mathcal{E}}_\ell(u, \alpha) = \int_\Omega \widehat{W}(\varepsilon(u), \alpha) \, dx + \int_\Omega G_c \mathcal{S}_\ell(\alpha), \tag{34}$$

where

$$\widehat{W}(\varepsilon, \alpha) = \kappa_0 \frac{\text{tr}^-(\varepsilon)^2}{2} + (a(\alpha) + k_\ell) \left(\kappa_0 \frac{\text{tr}^+(\varepsilon)^2}{2} + \mu \varepsilon_D \cdot \varepsilon_D \right). \tag{35}$$

With (34) only the strain energy associated to expansion and shear enters into the competition with the surface energy. In the regions where the volume change is negative, the spherical part of the strain energy cannot be released by the creation of new cracks. On the contrary, in the regions with positive volume change, the whole elastic energy may redeem the increments of the surface energy. These properties modify the criterion for crack propagation underlying the energy minimality principle. As a result, the new functional assures a residual resistance in compression, without forbidding crack opening. A similar damage criterion is adopted in the damage models of Comi (2001) and Ramtani et al. (1992). The hope that the proposed regularized formulation leads to the unilateral contact model in the limit $\ell \rightarrow 0$ is corroborated by the fact that $\widehat{\mathcal{E}}_\ell(u, \alpha)$ reduces to (22) in regions with a positive volume change and to (31) in regions with a negative volume change.

4.4. Uniaxial homogeneous response

Consider a volume element in an uniaxial stress state, say $\sigma = \sigma_{33} e_3 \otimes e_3$, with imposed axial strain ε_{33} . To illustrate the properties of the regularized formulation as a gradient damage model, we study the uniaxial homogeneous material response. This is obtained by minimizing the functional (34) under the hypothesis $\nabla \alpha = 0$ (homogeneous damage distribution). We focus on the case without residual stiffness ($k_\ell = 0$).

At the i th loading step, the minimization of the regularized functional with respect to $\alpha \geq \alpha_{i-1}$ gives the Kuhn–Tucker conditions representing the damage criterion (see e.g. Lorentz and Andrieux, 1999). With $\nabla \alpha = 0$, they are in the form

$$f(\sigma_{33}, \alpha) \geq 0, \quad \alpha - \alpha_{i-1} \geq 0, \quad f(\sigma_{33}, \alpha)(\alpha - \alpha_{i-1}) = 0, \tag{36}$$

where, for the unilateral contact model (34), if $\varepsilon_{33} \geq 0$

$$\sigma_{33} = a(\alpha) Y \varepsilon_{33}, \quad f(\sigma_{33}, \alpha) = \frac{\sigma_{33}^2 a'(\alpha)}{2a(\alpha)^2 Y} + \frac{G_c W'(\alpha)}{\ell}, \tag{37}$$

whilst if $\varepsilon_{33} \leq 0$

$$\sigma_{33} = \frac{3a(\alpha)}{2(1+\nu) + a(\alpha)(1-2\nu)} Y \varepsilon_{33}, \quad f(\sigma_{33}, \alpha) = \frac{\sigma_{33}^2 a'(\alpha)(1+\nu)}{3a(\alpha)^2 Y} + \frac{G_c W'(\alpha)}{\ell}. \tag{38}$$

Solving (36)–(38) for σ_{33} and α as a function of ε_{33} starting from $\varepsilon_{33} = 0$, with either monotonically increasing or monotonically decreasing loadings, gives the uniaxial strain–stress relationship and the damage evolution. Fig. 2 reports

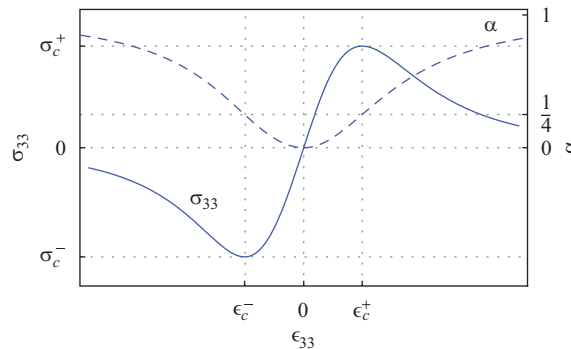


Fig. 2. Uniaxial homogeneous response for the regularized unilateral contact model given by (34) with $w(\alpha) = \alpha^2/4$ and $a(\alpha) = (1 - \alpha)^2$: stress σ_{33} (continuous line) and damage parameter α (dashed line) as a function of the axial strain ε_{33} . See Eqs. (39) and (40) for the expression of ε_c^\pm and σ_c^\pm , respectively.

the results obtained for $a(\alpha) = (1 - \alpha)^2$ and $w(\alpha) = \alpha^2/4$, as assumed in (25). The diagram of Fig. 2 illustrates some important mechanical properties of such a regularized formulation as a gradient damage model:

- The model does not have a purely elastic phase. With (25), $w'(0) = 0$ and the limit of elasticity of the underlying damage model is zero. The strain–stress diagram shows a hardening phase from $\epsilon_{33} = 0$ to $\epsilon_{33} = \epsilon_c^+$ (or ϵ_c^-), followed by a softening phase for $\epsilon_{33} > \epsilon_c^+$ (or $\epsilon_{33} < \epsilon_c^-$) where the critical strains are

$$\epsilon_c^+ = \sqrt{\frac{G_c}{6Y\ell}}, \quad \epsilon_c^- = -\frac{41 + 14\nu}{96\sqrt{1+\nu}}\sqrt{\frac{G_c}{Y\ell}} \quad (39)$$

- There are maximum allowable values of the stress for homogeneous states, σ_c^+ in uniaxial traction and σ_c^- in uniaxial compression. Their values are computed to be

$$\sigma_c^+ = \frac{3}{16}\sqrt{\frac{3}{2}}\sqrt{\frac{YG_c}{\ell}}, \quad \sigma_c^- = -\frac{9}{32\sqrt{1+\nu}}\sqrt{\frac{YG_c}{\ell}}. \quad (40)$$

The critical values of the stress are reached at $\epsilon_{33} = \pm\epsilon_c$. The smaller the internal length, the higher the maximum allowable stress.

- The material response is not symmetric in traction and compression. In particular, the limit values of the stress in (40) differ by a factor $\sqrt{2(1+\nu)}/3$.
- The uniaxial response of Fig. 2 may be interpreted as the homogeneous solution for the traction/compression test of a bar. In a quasi-static evolution ruled by a local minimality condition, the homogeneous response is stable provided that the length of the bar is small enough, as shown in Benallal and Marigo (2007). For long bars, the system will follow the response in Fig. 2 till $|\epsilon| < \epsilon_c$, snapping to a non-homogeneous solution (the cracked state) at ϵ_c . In any case, the bar cannot sustain a stress greater than σ_c^+ . Hence σ_c^+ may be regarded as the rupture stresses in the traction/compression test. The small differences between the critical values in traction and in compression are not in agreement with the experimental results. This point motivates the use of more complex damage models to reproduce a realistic material behavior (see e.g. Comi, 2001; Badel et al., 2007).

The properties above are specific for $w(\alpha)$ and $a(\alpha)$ as in (25), which represents a particular choice of the constitutive properties of the damage model. This is not the unique choice assuring the gamma-convergence of the regularized functional toward brittle fracture for $\ell \rightarrow 0$ (see Braides, 1998). For example, an interesting alternative damage model is obtained by choosing

$$a(\alpha) = (1 - \alpha)^2, \quad w(\alpha) = c\alpha, \quad (41)$$

where c is a suitable normalization constant. In this case, the homogeneous model would be characterized by a non-vanishing elastic phase, because $w'(0) \neq 0$ (see Eqs. (37) and (38)).

4.5. Choice of the length ℓ : brittle fracture vs. gradient damage

The shape of the damaged zone (and hence of the approximate crack path) can significantly change with the length ℓ if ℓ is not sufficiently small with respect to the size L of the domain Ω . The value of ℓ may be chosen according to two criteria, depending on whether ℓ is considered as a pure numerical parameter of the regularized model of brittle fracture or as a real material parameter of a gradient damage model.

In the former case, the smaller ℓ the better the approximation of the brittle fracture model by a gradient damage model. But the improvement of the approximation will have a cost, because the mesh size must be smaller than ℓ . Hence, it is of practical importance to determine from which value of ℓ/L the results become stable. At the present time, that determination is purely empirical. Our numerical tests presented in the following sections use ℓ/L of the order of $\frac{1}{100}$.

In the latter case, the value of ℓ must be selected according to experimental data. A possible way is to identify the maximum allowable stress in the uniaxial homogeneous response σ_c^+ given (40) with the rupture stress σ_c in uniaxial traction tests of a bar. Using the available database values for the Young modulus Y , the toughness G_c , and the rupture stress σ_c , it is then possible to uniquely determine a reasonable value for the internal length ℓ . When ℓ is fixed, there are no more free numerical parameters, but the damaged zone can depend on the size L of the structure. That will correspond to a real size effect, well known for non-local damage models. In return, if the numerical results become stable when L becomes large enough, then we can conclude that the size effects disappear for large structures and that we recover the results corresponding to a brittle material of toughness G_c .

5. Numerical implementation

The numerical solution of the regularized minimization problems described in the previous section is not a trivial task because the regularized functionals are not convex in the pair (u, α) . Solving numerically the global optimization problem is

not feasible. One may try at best to look for local minima. To this end, Bourdin et al. (2000), dealing with the model with no-contact condition, used an iterative algorithm based on an alternate minimization strategy on (u, α) . Lancioni and Royer-Carfagni (2009) and Del Piero et al. (2007) applied the same basic algorithm to solve the problem for the shear fracture model and for the fracture of a non-linear elastic body, respectively. Also our numerical work on the unilateral contact model is based on an alternate minimization. We recall below the main points of the algorithm, focusing on the difficulties in the solution of the two basic subproblems due to the unilateral contact and the irreversibility condition. Finally, we discuss the finite element implementation and the criteria for a correct tuning of the key numerical parameters.

5.1. The minimization algorithm

5.1.1. Alternate minimization

The alternate minimization algorithm consists in solving a series of minimization subproblems on u at fixed α , and vice versa on α at fixed u , until convergence. The effectiveness of this strategy relies on the convexity and coerciveness of $\mathcal{E}_\ell(u, \alpha)$ in each of the two variables. On the basis of the knowledge of the solution (u_{i-1}, α_{i-1}) at the time step t_{i-1} , the solution (u_i, α_i) at time step t_i , defined as the solution of (26), is found by the following iterative procedure:

- Initialization: Set $(u^{(0)}, \alpha^{(0)}) := (u_{i-1}, \alpha_{i-1})$.
- Iteration p :

1. Compute, under the constraint $u(x) = t_i \bar{U}(x)$ on $\partial_u \Omega$,

$$u^{(p)} := \underset{u}{\operatorname{argmin}} \mathcal{E}_\ell(u, \alpha^{(p-1)}). \tag{42}$$

2. Compute, under the constraints $\alpha_{i-1} \leq \alpha \leq 1$ on Ω ,

$$\alpha^{(p)} := \underset{\alpha}{\operatorname{argmin}} \mathcal{E}_\ell(u^{(p)}, \alpha). \tag{43}$$

- End: Repeat until $\|\alpha^{(p)} - \alpha^{(p-1)}\|_\infty \leq \delta_1$. Set $(u_i, \alpha_i) := (u^{(p)}, \alpha^{(p)})$.

This algorithm imposes the solution to satisfy only first order optimality conditions on u and α . To ensure that its output is a local minimum, further tests based on second order optimality conditions should be performed. This point is currently under investigation but not included in the present work. Of course, global optimization remains out of reach.

5.1.2. Minimization at fixed α

In the model with no-contact condition and in the shear fracture model, the energy functional is quadratic in u and the substep (42) reduces to the solution of a linear system. In the unilateral contact model, $\widehat{\mathcal{E}}_\ell(u, \alpha)$ is not any more quadratic in u . At fixed α , $\widehat{\mathcal{E}}_\ell(u, \alpha)$ is a continuous, piecewise quadratic, *strictly convex* functional of u , with a continuous first derivative. The associated minimization subproblem (42) is non-smooth, but it enjoys existence and uniqueness of the solution. To solve it, we apply the following quasi-Newton algorithm:

- Initialization: Set $u^{(p,0)} := u^{(p-1)}$.
- Iteration q : Compute, under the constraint $u(x) = t_i \bar{U}(x)$ on $\partial_u \Omega$,

$$u^{(p,q)} := \underset{u}{\operatorname{argmin}} \mathcal{K}(u^{(p,q-1)}, \alpha^{(p-1)})(u), \tag{44}$$

where the stiffness operator \mathcal{K} is defined by

$$\mathcal{K}(u, \alpha)(v) := \int_\Omega \kappa_0 (1 - H(\operatorname{div} u)) (\operatorname{div} v)^2 \, dx + \int_\Omega (a(\alpha) + k_\ell) (\kappa_0 H(\operatorname{div} u) (\operatorname{div} v)^2 + 2\mu \varepsilon_D(v) \cdot \varepsilon_D(v)) \, dx. \tag{45}$$

H being the Heaviside step function defined as $H(x) = 1$ if $x \geq 0$, $H(x) = 0$ if $x < 0$.

- End: Repeat until $\|u^{(p,q)} - u^{(p,q-1)}\|_\infty \leq \delta_2$ with $\delta_2 < \delta_1$. Set $u^{(p)} := u^{(p,q)}$.

The stiffness operator \mathcal{K} coincides with the second directional derivative of $\widehat{\mathcal{E}}_\ell(u, \alpha)$ with respect to u when the latter exists, i.e. when $\operatorname{div} u \neq 0$ almost everywhere. Although the global convergence of such undamped Newton algorithm is not assured in general, its application to non-smooth problems is not foolish, as argued by Alart (1997). In all our simulations we observed a quick convergence, normally in two or three iterations, provided that the residual stiffness k_ℓ is sufficiently high to ensure a reasonable conditioning of the tangential stiffness matrix. On the other hand, numerical instabilities caused by bad-conditioning problems may arise if k_ℓ is too small. This issue is not due to the nonlinearities in u , because

the shear fracture model presents the same basic problem, even if in that case the minimization at fixed α consists in the solution of a single linear system (see the comments in Section 5.2).

5.1.3. Minimization at fixed u

The minimization on α for fixed u in (43) is a quadratic optimization problem with bound constraints. The unconstrained minimizers of the functional with $a(\alpha)$ and $w(\alpha)$ given in (25), automatically satisfy the upper bound $\alpha \leq 1$. The main difficulty stays behind the numerical implementation of the irreversibility condition $\alpha \leq \alpha_{i-1}$. The previous numerical works in the literature avoid the recourse to bound-constrained optimization algorithms and reduce the minimization in α to the solution of an unconstrained linear system. Bourdin et al. (2000) use an approximate version of the irreversibility condition to transform the lower bound on α into an equality constraint. They remove the lower bound on α and impose $\alpha = 1$ in the regions where the solution of the previous type step α_{i-1} is sufficiently close to 1. In other words, they prevent material healing only for fully developed cracks. Lancioni and Royer-Carfagni (2009) replace the substep 2 of the alternate minimization algorithm by the following two substeps. The irreversibility condition is enforced projecting the solution of the unconstrained problem on the admissible space:

- 2(a) Solve (43) on α at fixed u without bound constraints. This reduces to the solution of a linear system.
- 2(b) Set $\alpha = \alpha_{i-1}$ wherever the obtained solution for α is smaller than its local value α_{i-1} at the previous time step.

Such a *a posteriori* projection procedure keeps the exact version of the irreversibility conditions $\alpha \geq \alpha_{i-1}$, but deviates from a true alternate minimization algorithm. The solution for α obtained at the end of each iteration does not coincide necessarily with the minimum of the constrained problem. Allaire et al. (2007) adopt the same solution scheme to account for the irreversibility condition in the simulation of a damage evolution by a level set method. Del Piero et al. (2007) use a combination of the two approximations above, by implementing the irreversibility condition as in Lancioni and Royer-Carfagni (2009), but only wherever α exceeds a fixed threshold, as in Bourdin et al. (2000).

In our numerical implementation of the alternate minimization algorithm, we tried to keep the exact version of the irreversibility condition in a true alternate minimization scheme. To this end, we had recourse to a solver for large-scale bound-constrained optimization. Especially, we employed the solver included in the Optimization Toolbox of Matlab, which implements the reflective Newton trust-region algorithm described in Coleman and Yuying (1996). For all the considered test cases, we compared the results obtained with the bound-constrained solver to those obtained with the projection method employed by Lancioni and Royer-Carfagni. We did not note any discrepancy in the final crack patterns and energy diagrams. The fundamental advantage of the projection method is to require the solution of a single linear system, a task for which standard reliable solvers may be used. However, the overall algorithm using the *a posteriori* projection is not any more a genuine alternate minimization. On the other hand, using solvers for large-scale bound-constrained optimization at each step of the alternate minimization is extremely expensive in terms of computational costs.

5.2. Discretization and parameter setting

To obtain a discretized formulation of the minimization problem, we use standard linear triangular finite elements with unstructured and uniform meshes. In 2-D elasticity, each element has three nodal degrees of freedom: the two components of the displacement vector and α . The key parameters to be set for a numerical simulation are the regularization parameter ℓ , the typical element size, say h , the loading increment ΔT , and the residual stiffness k_ℓ . The loading increment ΔT , which we keep uniform, may be adapted to follow the phenomena encountered in each simulation.

An accurate estimation of the discretized surface energies requires the element size h to be much smaller than the regularization parameter ℓ . Namely, Bourdin et al. (2008) show that, with linear triangular elements the surface energy is overestimated by a factor $f(h/\ell) = 1 + h/4\ell$. Having $h/\ell \ll 1$ demands the use of extremely large meshes, because ℓ must be sufficiently small to make the regularized formulation a good approximation of brittle fracture. Numerical experiments show that setting $h \sim \ell$ still gives qualitatively reasonable results, even if the computed surface energy must be expected to be correspondingly overestimated.

The dependence of the estimated surface energy on the mesh size rules also that the mesh must be kept uniform to avoid artificial inhomogeneities. Similarly, structured meshes introduce anisotropies, as pointed out by Negri (1999). This suggests to avoid adaptive mesh refinement, even if this option is attractive to reduce the computational cost.

The residual stiffness k_ℓ must be chosen sufficiently small to not add a large artificial stiffness to damaged elements; at the same time, it must be sufficiently large to assure a reasonable conditioning of the stiffness matrix used for the solution of the minimization subproblem at fixed α . In the model without contact condition this choice is not critical. Even with extremely small values of k_ℓ (e.g. $k_\ell \sim 10^{-9}$), we never observed numerical instabilities in the solution of the linear system obtained as minimality condition at fixed α . On the other hand, the shear fracture model and the unilateral contact model are much more sensitive to the choice of the residual stiffness. We observed numerical instabilities starting from $k_\ell \sim 10^{-5}$. Similar issues have been put into evidence also in the shear fracture model of Lancioni and Royer-Carfagni (2009) and in the model with geometrical and material non-linearities of Del Piero et al. (2007). The shear fracture model and the

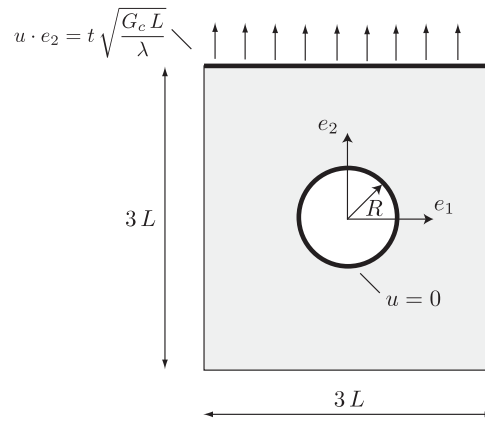


Fig. 3. Fiber reinforced matrix: geometry and boundary conditions.

unilateral contact model show the same basic problem, which is associated to the presence of compressed fracture in shear. A plausible explanation is that shear fractures in compression include elements characterized by a vanishing stiffness in purely deviatoric modes and a finite stiffness with respect to volume changes. This induces a bad-conditioning in the solution of the displacement problems at fixed α . The issue seems similar to the one encountered in incompressible elasticity (see e.g. Hughes, 2000). Possible remedies to be explored in future works include the use of higher order finite elements with special reduced integration techniques and augmented Lagrangian methods (Glowinski and Le Tallec, 1982). In the present work, we obtained reasonable results using a trade-off value for the residual stiffness, $k_\ell \sim 10^{-4}$.

The regularized functionals introduced in Section 4 underestimate the surface energy of fracture developing at the boundaries. To recover a correct value for the surface energy, Bourdin et al. (2000) and Del Piero et al. (2007) performed the computations on an enlarged logical domain. Here, we bypass the problem by forbidding fractures to develop exactly at the boundary. To this end we impose as boundary condition $\alpha = 0$ on $\partial\Omega$. For small ℓ , this constraint has a minor influence on the results because fractures are free to appear at a small distance from the boundaries whenever it turns out to be beneficial for energy minimization. This point is well illustrated by the numerical results in the next section. The final effect is similar to covering the boundary by a non-breakable film, whose thickness goes to zero as $\ell \rightarrow 0$. The resulting additional residual stiffness reduces the bad-conditioning problems encountered when a compressed shear fracture meets a boundary.

6. Numerical experiments

Section 4 introduces a tentative regularized formulation for the variational model including the unilateral contact condition without giving any rigorous convergence proof toward the desired limit behavior. The efficiency of the regularized functional in reproducing fractures with unilateral contact will be illustrated through numerical simulations. To this end we revisit two examples of 2-D elasticity considered in the literature by comparing the results of the different contact models: no-contact, shear, and unilateral.

The numerical values will refer to non-dimensional variables. For the considered models, a dimensional analysis shows that the values of the typical material stiffness, say the Lamé coefficient λ , the fracture toughness G_c , and the scaling length L can be factored out from the energy functional by scaling the displacement with $u_0 = \sqrt{G_c L / \lambda}$. Only two non-dimensional parameters influence the results of the numerical simulations: the ratio of the Lamé coefficients μ/λ (or equivalently the Poisson coefficient ν) and the ratio ℓ/L between the regularization parameter and the typical geometric dimension.

6.1. Fiber reinforced matrix

The first example is a model problem introduced in Bourdin et al. (2000) to highlight the ability of the variational approach to recover initiation phenomena and complex crack patterns. It has been revisited also in Del Piero et al. (2007) with a model including non-linear effects and in Bourdin (2007) using a backtracking algorithm. Fig. 3 represents the system geometry, a squared plate of side $3L$ with a circular blocked inclusion of radius $R = \rho L$. The loading is given by applied normal² displacements $u \cdot e_2 = t u_0$ on the upper border of the plate. The other boundaries are free. This setup may stand for the traction/compression experiment of a fiber reinforced matrix, or the failure test of a pinned plate (see e.g. Naik and Prabhakaran, 1987).

² Differently from Del Piero et al. (2007), the tangential displacements are left free.

Our simulations refer to the case $\lambda = \mu$ with plane strain assumptions, corresponding to $\nu = 0.25$, and $\ell/L = \frac{1}{100}$. For the discretization, we adopted a non-structured homogeneous finite element mesh composed of 182 580 triangles with a total number of $3 \times 92\,047$ degrees of freedom. The typical element size is about $h \sim 0.01L$. For the residual stiffness, we set $k_r = 2 \times 10^{-4}$. In the simulations discussed below, the loading increment is $\Delta T = 0.05$. Numerical results show an interesting dependence on the geometric aspect ratio, specified by the radius of the inclusion. We report on the cases where $\rho = 0.5$ and 0.25.

6.1.1. Case 1: $\rho = 0.5$

Figs. 4 and 5 summarize the results obtained with the unilateral contact model for traction ($t > 0$) and compression ($t < 0$) loadings. The images at the top display the evolution of the deformed configuration of the structure colored according to the values of α . A linear scale ranging from $\alpha = 0$ (black) to $\alpha = 1$ (white) is used. As expected, α is close to zero almost everywhere except in thin bands with thickness of the order of ℓ . Those bands are the regularized representation of the cracks. Elements with $\alpha > 0.95$ are considered completely cracked and are not represented. The images at the bottom report on the undeformed geometry the sign of the volume change in each element, according to the value of the divergence of the displacement field. Light gray stays for compressed regions ($\text{div}(u) < 0$), dark gray is for expanded regions ($\text{div}(u) > 0$). Here the coloring of the cracked elements ($\alpha > 0.95$) distinguishes between opening cracks with a total release of the elastic energy (in white) and shear cracks releasing only the deviatoric part of the elastic energy (in black). This

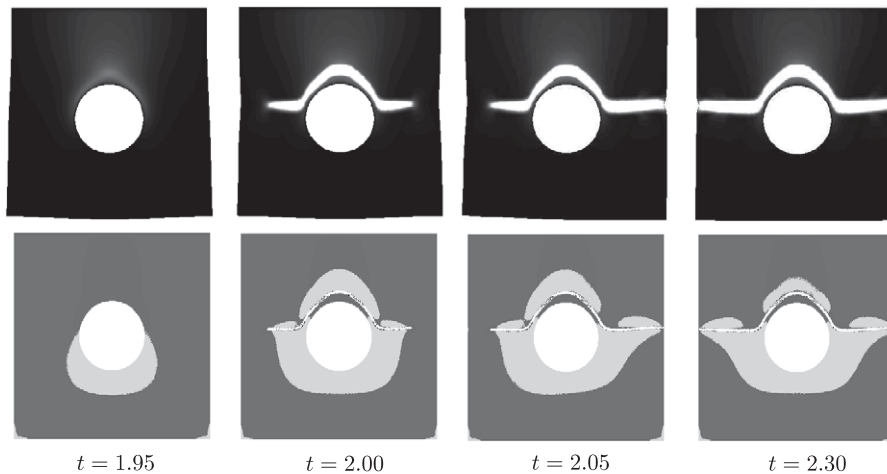


Fig. 4. Traction test with $\rho = 0.5$ using the unilateral contact model and the no-contact model, which give the same crack evolution. Top: damage field on the deformed configuration represented with a linear color scale ranging from black ($\alpha = 0$) to white ($\alpha = 1$). Bottom: regions with positive (dark gray) or negative (light gray) volume change and distinction between shear (in black) and opening (in white) cracks. In this case shear cracks are absent.

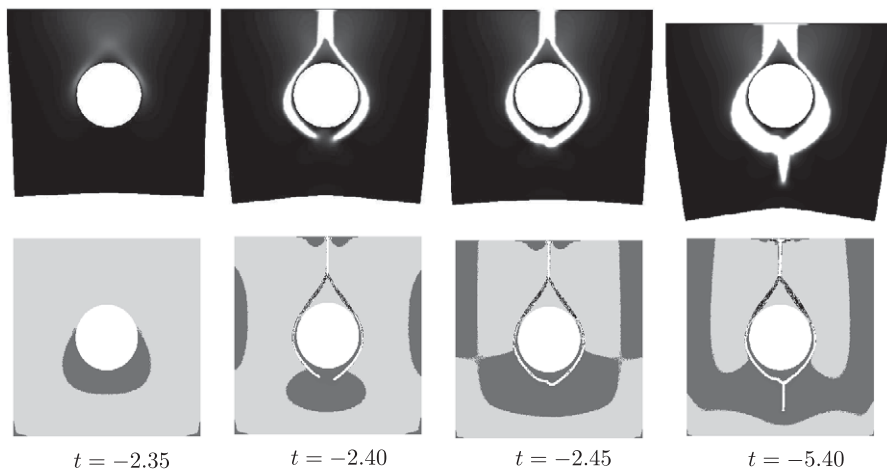


Fig. 5. Compression test for $\rho = 0.5$ using the unilateral contact model. Legend as in Fig. 4. The volume change diagrams (bottom row) underline the presence of shear cracks (in black).

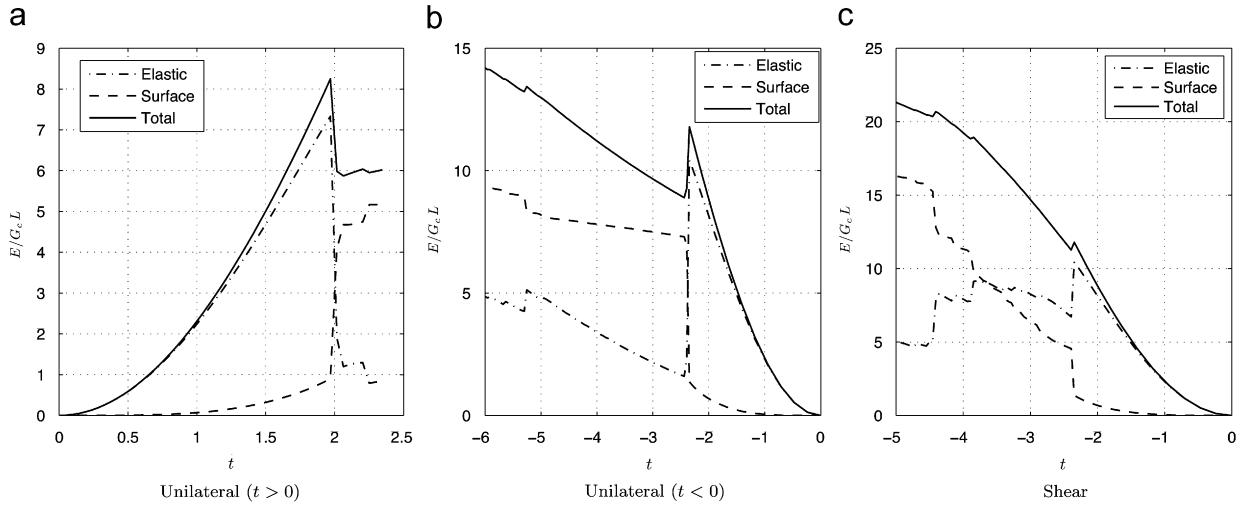


Fig. 6. Energy diagrams for the fiber reinforced matrix with $\rho = 0.5$ using the unilateral contact model and the shear fracture model. The no-contact model gives results identical to the unilateral model in traction (a).

representation helps understanding the behavior of the unilateral contact model, which strongly depends on the sign of the volume change.

Figs. 6(a) and (b) plot the elastic, surface, and total energies as a function of the loading parameter t , for $t > 0$ and $t < 0$, respectively. With the formulation of Francfort and Marigo (1998) based on global optimization at each time step, the total energy should be an absolutely continuous function of t . In our numerical results, the total energies are not continuous because the numerical algorithm of Section 5 does not implement global optimality conditions, but only local ones. With local minimization, a discontinuity in the total energy plot indicates a brutal phenomenon where the solution at the previous step becomes unstable and the structure snaps to a new cracked state at a lower energy level. The associated critical value of the loading parameter may depend on the length ℓ , as for the example of Section 4.4. To recover the continuity of the total energy and quasi-static evolutions coherent with Francfort and Marigo (1998), Bourdin (2007) proposes a specific backtracking algorithm, which is not applied here.

For the traction test (Fig. 4), the unilateral contact model gives the same results as the no-contact model, which are reported in Bourdin et al. (2000). The discontinuities in the energy diagrams of Fig. 6(a) distinguish brutal events. Cracks develop only in regions with positive volume change. We observe a brutal initiation phenomenon at $t \sim 2.00$, followed by an asymmetric collapse of one of the two residual ligaments and the final failure. A more detailed description of the time history may be obtained by further refining the time increment, but this is inessential for the present study. Analogue behaviors have been widely commented in several works (Bourdin et al., 2000, 2008; Bourdin, 2007; Del Piero et al., 2007). A careful check of the final crack pattern at $t = 2.30$ reveals the persistence of thin undamaged films, which is due to the boundary condition $\alpha = 0$ adopted in our numerical work. This does not affect the final result.

Reversing the loading ($t < 0$), the quasi-static evolution of the model with no-contact conditions remains as in Fig. 4 but with a reversed sign of the displacement. This implies an unphysical interpenetration of the crack lips. On the other hand, the proposed regularized formulation accounting for the unilateral contact condition shows a completely different behavior (Fig. 5):

- The (almost) elastic solution remains stable until $t \sim -2.35$.
- At $t \sim -2.40$ a brutal initiation phenomenon generates a complex crack pattern, including branches of shear and opening cracks, represented, respectively, in black and in white in the volume change diagrams.
- At $t \sim -2.45$ the branches coming from the left and the right of the inclusion rejoin at the bottom. Although the crack now isolates the inclusion from the rest of the structure, there is still an important residual elastic energy due to unilateral contact effects, as shown by the energy diagram of Fig. 6(b).
- At $t \sim -5.40$ we observe a further brutal event with the appearance of a new opening crack at the bottom of the inclusion. This crack seems to continue propagating at a slower time scale. Our simulation stops before the expected complete separation of the solid in two parts.

Fig. 7 shows the crack patterns obtained with the shear fracture model. The corresponding energy plots are in Fig. 6(c). In this case, all the cracks are of the shear type with a partial release of the elastic energy. Forbidding *a priori* the crack opening and the release of the isotropic part of the elastic energy has important consequences on the crack propagation

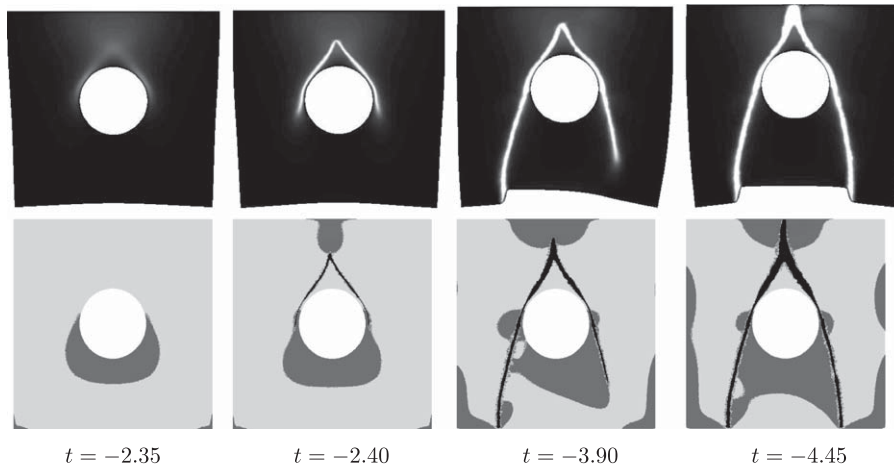


Fig. 7. Compression test for $\rho = 0.5$ using the shear fracture model.

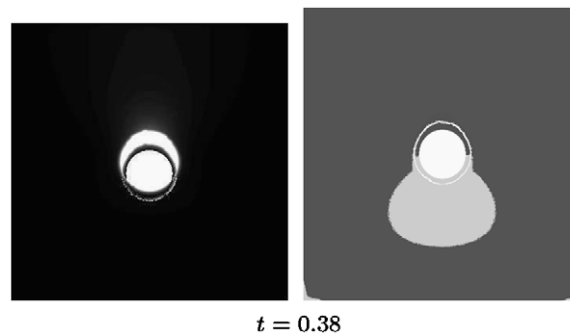


Fig. 8. No-contact model: traction test for $\rho = 0.25$. The crack in the compressed region (light gray) implies material interpenetration.

criterion. As for the no-contact model, the results of the traction and compression tests coincide, modulo the sign of the displacement field.

With the adopted dimensional scaling, the values of the surface energy in the energy plots of Fig. 6 should correspond to the non-dimensional lengths of the cracks of Fig. 4. Considering that the numerical results are obtained with a typical element size $h \sim \ell$, we may expect an overestimation of the surface energy by a factor $f(h/\ell) = 1 + h/4\ell \sim 1.25$ (see Bourdin et al., 2008, Section 8.1). This estimate is verified with a reasonable accuracy for the traction test of Fig. 4 characterized only by opening cracks. In the other cases including shear cracks, the computed surface energy is larger than the geometrical crack lengths. This is particularly evident for the shear model, where the computed surface energy in Fig. 6(c) appears to be approximately the double of the crack lengths in Fig. 7, even after accounting for the presumed corrective factor. The overestimation of the surface energy is highlighted also by the increased thickness of the damaged bands. This issue, for which we do not have a satisfying explication, deserves further investigations. We suspect it may be related to the relatively high residual stiffness and the bad-conditioning problems encountered in regions with shear cracks.

6.1.2. Case 2: $\rho = 0.25$

For small values of the inclusion radius ρ , the surface energy required to tear the plate apart by a circular crack around the inclusion becomes smaller than the surface energy required to cut the plate transversally as in Fig. 4. The circular crack pattern is indeed the result of the model with no-contact condition for a fiber radius $\rho = 0.25$, as already reported in Bourdin et al. (2000). However, the final result of the traction test recalled in Fig. 8 clearly shows material interpenetration in the compressed region at the bottom of the inclusion.

Del Piero et al. (2007) run the same simulation using a non-linear model that precludes material interpenetration by a suitable non-linear constitutive law penalizing large volume changes. The crack shape they found is similar to the one of the no-contact model, but without crack interpenetration and a diffuse damage in the compressed region. The associated rupture mechanism remains of difficult interpretation.

Our model for unilateral contact provides the solution in Fig. 9. Its explanation is clear: by forbidding crack interpenetration, circular crack patterns around the fiber are ruled out from the set of admissible cracks; the cracking mode

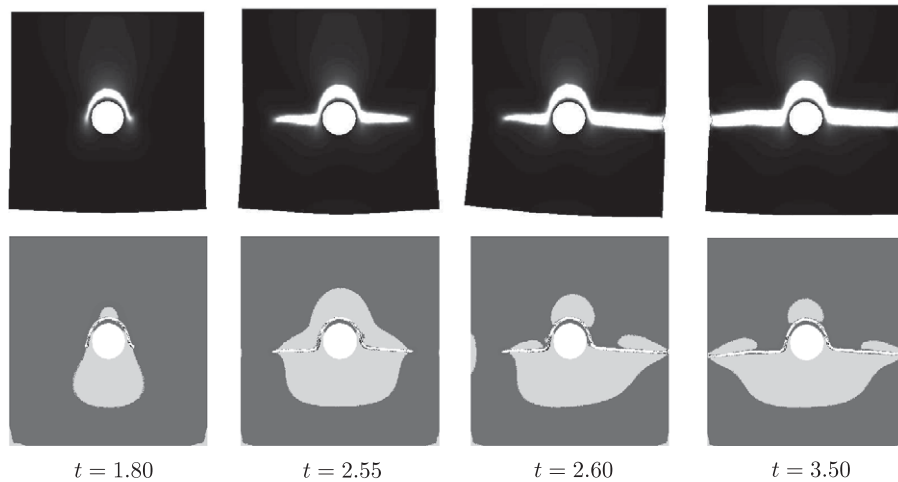


Fig. 9. Unilateral contact model: traction test for $\rho = 0.25$.

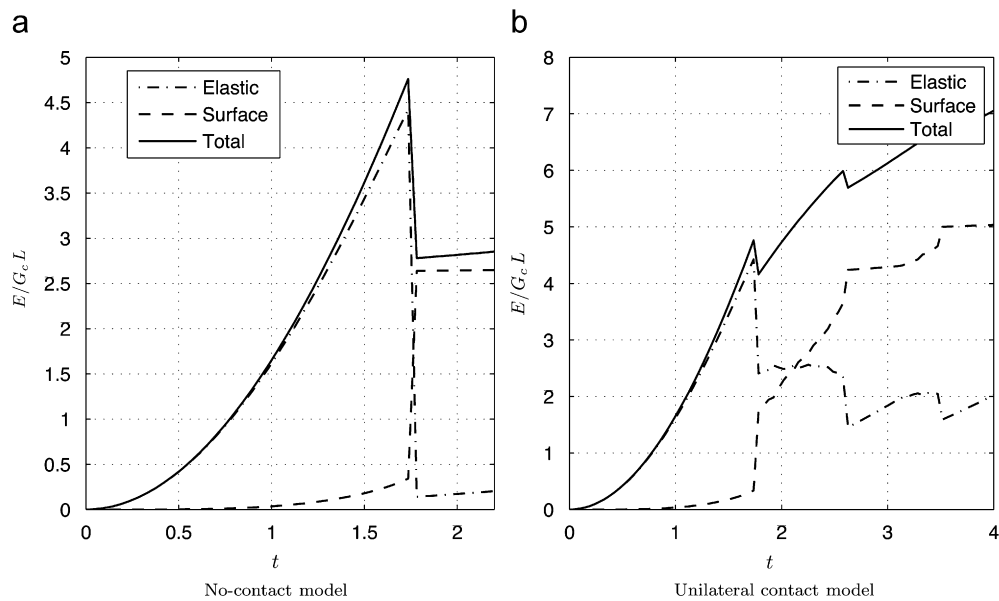


Fig. 10. Energy diagrams for $\rho = 0.25$ (traction).

with minimal energy continues to be similar to the one obtained for inclusions of a larger radius. For the compression test, not reported here, we observed results qualitatively similar to those of Fig. 5.

Fig. 10 compares the energy plots of the no-contact and the unilateral contact models.

6.2. Stone panel of the ashlar masonry of the French Panthéon

Lancioni and Royer-Carfagni (2009) propose an interesting application of the variational approach to fracture mechanics. They study the causes of the crack patterns observed in the stone panel of the ashlar masonry of the French Panthéon in Paris. They focus on a single stone panel with the simplified geometry reported in Fig. 11. The panel is modeled as a linear elastic isotropic solid with Poisson ratio $\nu = 0.1$ and plane stress conditions. The rectangular blocked inclusion simulates the effect of reinforcements in the form of iron staples. Using the shear fracture model, they obtain a crack pattern qualitatively similar to the one observed in situ with the loading mode of Fig. 11 (iron-staple pull-out). The study concludes that iron-staple pull-out is the most likely cause of the failure.

We re-run the simulation for the iron-staple pull-out test using a regularization parameter $\ell = 0.02L$, a residual stiffness $k_\ell = 2 \times 10^{-4}$, and a uniform mesh with typical element size $h = 0.01L$.

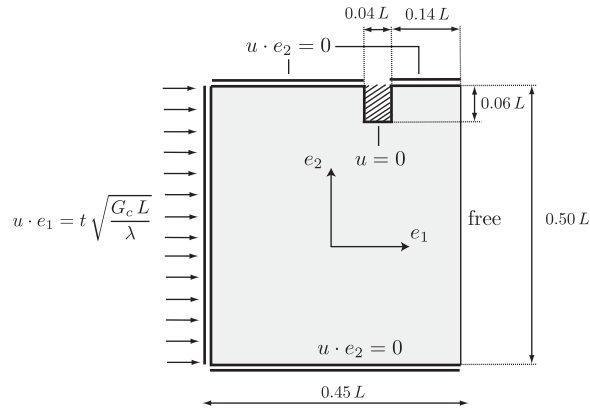


Fig. 11. A stone panel of the ashlar masonry of the French Panthéon. Geometry and boundary conditions are set as in Lancioni and Royer-Carfagni (2009) where $L = 1$ m. The blocked inclusion represents an iron-staple, the applied displacements simulates the structural loadings.

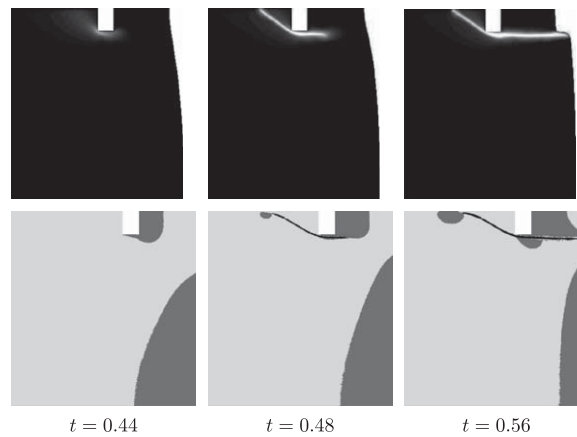


Fig. 12. Ashlar masonry of the French Panthéon. Iron-staple pull-out test for $t > 0$ with the shear fracture model.

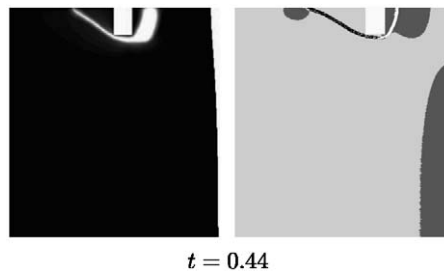


Fig. 13. Ashlar masonry of the French Panthéon. Iron-staple pull-out test for $t > 0$ with the unilateral contact model. Deformed configuration (left) and volume change diagram (right). The whole crack, including shear and opening branches, appears after a single brutal event at $t \sim 0.44$.

With the shear fracture model, we obtained the evolution in Fig. 12, which is in agreement with the results of Lancioni and Royer-Carfagni (2009). At $t \sim 0.48$ a shear crack appears at the left of the blocked inclusion. It continues propagating toward the free border, reached at $t \sim 0.56$.

The unilateral contact model gives a different result, which is resumed in Fig. 13. Removing the hypothesis that cracks can propagate only in shear mode, we observe an opening crack in the region at the right of the inclusion subjected to a positive volume change. This crack pattern allows the system to reach a state at a significantly lower energy level, as pointed out by the energy diagrams of Fig. 14.

For reverse loadings ($t < 0$), the crack pattern given by the shear fracture model is the same as in Fig. 12, with an opposite sign of the displacements. The model with unilateral contact provides the solution in Fig. 15. The crack pattern is again different from the one of the shear model.

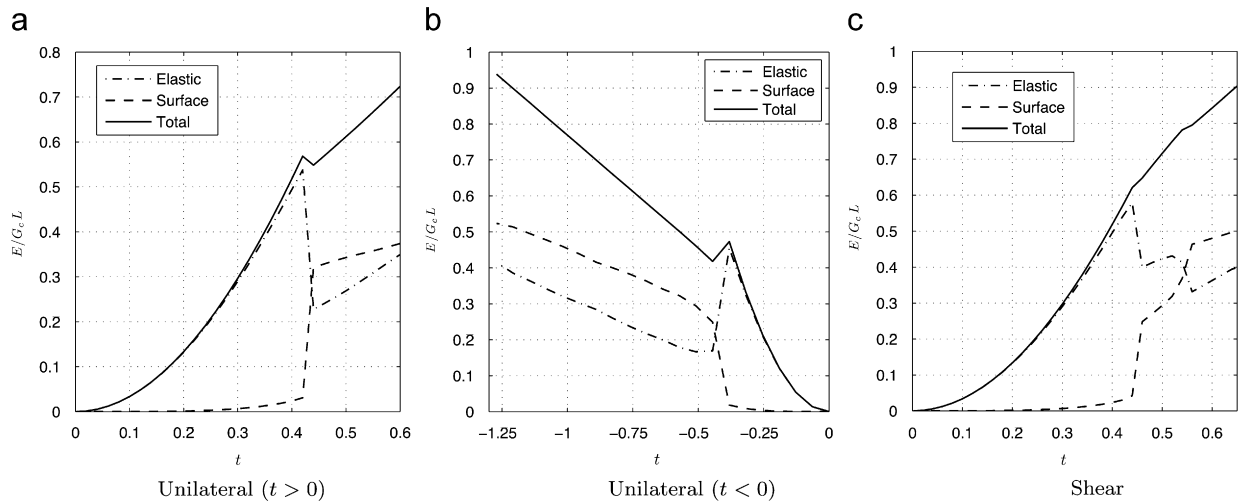


Fig. 14. Energies for Panthéon ashlar masonry: traction (a) and compression (b) with the unilateral contact model are compared to the shear fracture model (c).

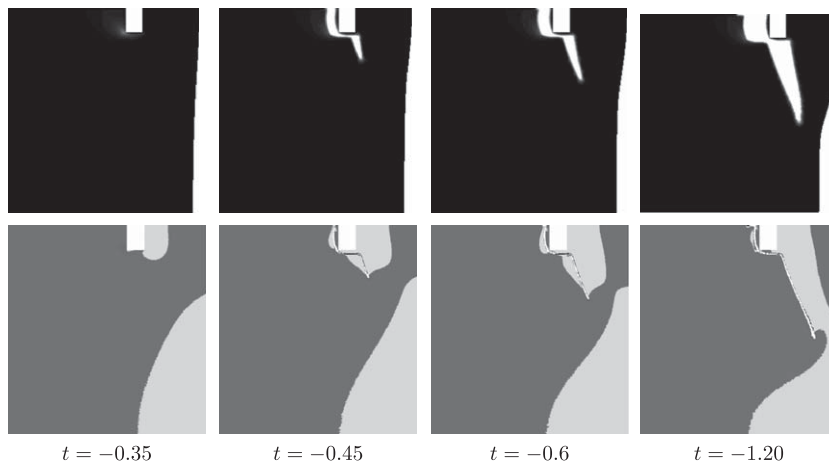


Fig. 15. Ashlar masonry of the French Panthéon. Iron-staple pull-out test for $t < 0$ using the unilateral contact model.

A close look to Fig. 15 enlightens an interesting feature of the proposed model: a crack generated in shear may change type during the evolution, becoming an opening crack with a total release of the elastic energy (and vice versa). In the present case, the horizontal branch of the crack at the bottom of the inclusion appears as a shear crack with partial release of the elastic energy at $t = -0.45$ (in black in the bottom row of images). It switches to the opening mode at $t = -1.20$ (in white in the bottom row of images) giving a total release of the elastic energy. This property, which is barely appreciable in the present simulation, may be fundamental to reproduce a realistic physical behavior for more complex loading cases (e.g. cyclic loadings).

The reported results may provide further support to the study of Lancioni and Royer-Carfagni on the damage of the Panthéon ashlar masonry. Observing that the final crack pattern given by the shear fracture model (Fig. 12) is in qualitative agreement to the one observed experimentally, they conclude that the loading mode in Fig. 11 is the most probable cause of failure. The more realistic model with unilateral contact show that such a loading mode alone would probably induce a different failure pattern including opening cracks. At the light of the information reported in Lancioni and Royer-Carfagni (2009) and our results, we suspect that the crack pattern observed *in situ* can be coherently justified only considering the combined action of multiple loadings, including compressive forces directed along the vertical direction e_2 . Example of such additional loadings may be the staple expansion due to oxidation considered in Lancioni and Royer-Carfagni (2009). Another point to be considered in future investigations is the adherence of the stone panel to the substrate.

7. Concluding remarks

Starting from the regularized model proposed by Bourdin et al. (2000), separating the spherical part and the deviatoric part of the bulk energy and accounting for the sign of the volumetric strain, we have obtained a regularized model able to predict asymmetric results in traction and in compression. That constitutes a real improvement in comparison to the two previous models developed by Bourdin et al. (2000) and Lancioni and Royer-Carfagni (2009). Even though gamma-convergence results are unavailable at the present time, we believe that the new model is a good approximation of the non-interpenetration condition that must be satisfied by the crack lips. This feeling is reinforced by the realistic results of the various numerical tests presented above. Of course, all those numerical results are impacted by the choice of the alternate minimization algorithm the convergence of which to (local) minima is not guaranteed. Even if several numerical aspects remain to be improved, the variational approach to fracture and its regularized versions are a very powerful tool to predict intricate crack paths without any *a priori* assumption.

Acknowledgments

The present work has been developed in the framework of the French research network MoMaS (Modélisations Mathématiques et Simulations numériques liées aux problèmes de gestion des déchets nucléaires) and a collaborative research project with ONERA, the French Aerospace Lab (Programme Pluriannuel de Recherche Concerté en Durée de Vie). Their financial support is gratefully acknowledged. Moreover, we thank Blaise Bourdin and Antonin Chambolle for their constructive suggestions during the development of this work.

References

- Alart, P., 1997. Méthode de Newton généralisée en mécanique du contact. *J. Math. Pures Appl.* 76, 83–108.
- Allaire, G., Jouve, F., Van Goethem, N., 2007. A level set method for the numerical simulation of damage evolution. Internal Report 629, CMAP, Ecole Polytechnique.
- Ambrosio, L., Fusco, N., Pallara, D., 2000. *Functions of Bounded Variation and Free Discontinuity Problems*. Oxford Mathematical Monographs. Oxford Science Publications, Oxford.
- Ambrosio, L., Tortorelli, V., 1990. Approximation of functionals depending on jumps by elliptic functional via gamma-convergence. *Commun. Pure Appl. Math.* 43, 999–1036.
- Aranson, I., Kalatsky, V., Vinokur, V., 2000. Continuum field description of crack propagation. *Phys. Rev. Lett.* 85, 118–121.
- Babuska, I., Melenk, J., 1997. The partition of unity method. *Int. J. Numer. Methods Eng.* 40, 727–758.
- Badel, P., Godard, V., Leblond, J.B., 2007. Application of some anisotropic damage model to the prediction of the failure of some complex industrial concrete structure. *Int. J. Solids Struct.* 44, 5848–5874.
- Belletini, G., Coscia, A., 1994. Discrete approximation of a free discontinuity problem. *Numer. Funct. Anal. Optim.* 15, 201–224.
- Benallal, A., Marigo, J.-J., 2007. Bifurcation and stability issues in gradient theories with softening. *Modelling Simulation Mater. Sci. Eng.* 15, S283–S295.
- Bourdin, B., 2007. Numerical implementation of the variational formulation of quasi-static brittle fracture. *Interfaces Free Boundaries* 9, 411–430.
- Bourdin, B., Francfort, G., Marigo, J.-J., 2000. Numerical experiments in revisited brittle fracture. *J. Mech. Phys. Solids* 48, 797–826.
- Bourdin, B., Francfort, G., Marigo, J.-J., 2008. The variational approach to fracture. *J. Elasticity* 91, 5–148.
- Braides, A., 1998. Approximation of free-discontinuity problems. In: *Lecture Notes in Mathematics*, vol. 1694. Springer, Berlin.
- Camacho, G., Ortiz, M., 1996. Computational modelling of impact damage in brittle materials. *Int. J. Solids Struct.* 33, 2899–2938.
- Cazes, F., Coret, M., Combescure, A., Gravouil, A., 2009. A thermodynamic method for the construction of a cohesive law from a nonlocal damage model. *Int. J. Solids Struct.* 46, 1476–1490.
- Chambolle, A., 2003. A density result in two-dimensional linearized elasticity, and applications. *Arch. Ration. Mech. Anal.* 167, 211–233.
- Chambolle, A., 2004. An approximation result for special functions with bounded deformation. *J. Math. Pures Appl.* 83, 929–954.
- Ciarlet, P., Nečas, J., 1987. Injectivity and self-contact in nonlinear elasticity. *Arch. Ration. Mech. Anal.* 97 (3), 171–188.
- Coleman, T., Yuying, L., 1996. A reflective Newton method for minimizing a quadratic function subject to bounds on some of the variables. *SIAM J. Optim.* 6 (4), 1040–1058.
- Comi, C., 2001. A non-local model with tension and compression damage mechanisms. *Eur. J. Mech. A/Solids* 20, 1–22.
- Dal Maso, G., Francfort, G., Toader, R., 2005. Quasistatic crack growth in nonlinear elasticity. *Arch. Ration. Mech. Anal.* 176, 165–225.
- Dal Maso, G., Toader, R., 2002. A model for the quasi-static growth of brittle fractures: existence and approximation results. *Arch. Ration. Mech. Anal.* 162, 101–135.
- de Borst, R., Remmers, J., Needleman, A., Abellan, M.-A., 2004. Discrete vs smeared crack models for concrete fracture: bridging the gap. *Int. J. Numer. Methods Eng.* 28, 583–607.
- Del Piero, G., Lancioni, G., March, R., 2007. A variational model for fracture mechanics: numerical experiments. *J. Mech. Phys. Solids* 55, 2513–2537.
- Francfort, G., Larsen, C., 2003. Existence and convergence for quasi-static evolution in brittle fracture. *Commun. Pure Appl. Math.* 56 (10), 1465–1500.
- Francfort, G., Marigo, J.-J., 1998. Revisiting brittle fracture as an energy minimization problem. *J. Mech. Phys. Solids* 46 (8), 1319–1342.
- Giacomini, A., 2005. Ambrosio–Tortorelli approximation of quasi-static evolution of brittle fractures. *Calc. Var. Partial Differential Equations* 22, 129–172.
- Giacomini, A., Ponsiglione, M., 2008. Non-interpenetration of matter for SBV deformations of hyperelastic brittle materials. *Proc. R. Soc. Edinburgh Sect. A* 138 (5), 1019–1041.
- Glowinski, R., Le Tallec, P., 1982. Numerical solution of problems in incompressible finite elasticity by augmented Lagrangian methods (i): two-dimensional and axisymmetric problems. *SIAM J. Appl. Math.* 42, 400–425.
- Hakim, V., Karma, A., 2009. Laws of crack motion and phase-field models of fracture. *J. Mech. Phys. Solids* 57, 342–368.
- Hughes, J.T., 2000. *The Finite Element Method: Linear Static and Dynamic Finite Element Analysis*. Dover Publications, Mineola, NY.
- Ingraffea, A., Saouma, V., 1984. Numerical modelling of discrete crack propagation in reinforced and plain concrete. In: Sih, G., DiTommaso, A. (Eds.), *Fracture Mechanics of Concrete*. Martinus Nijhoff Publishers, Dordrecht, pp. 171–225.
- Jirasek, M., 1998. Nonlocal models for damage and fracture: comparison of approaches. *Int. J. Solids Struct.* 35, 4133–4145.
- Lancioni, G., Royer-Carfagni, G., 2009. The variational approach to fracture mechanics. A practical application to the French Panthéon in Paris. *J. Elasticity* 95, 1–30.
- Liebe, T., Steinmann, P., Benallal, A., 2001. Theoretical and computational numerical aspects of a thermodynamically consistent framework for geometrically linear gradient damage. *Comput. Methods Appl. Mech. Eng.* 190, 6555–6576.

- Lorentz, E., Andrieux, S., 1999. A variational formulation of nonlocal damage models. *Int. J. Plasticity* 15, 119–138.
- Lorentz, E., Benallal, A., 2005. Gradient constitutive relations: numerical aspects and applications to gradient damage. *Comput. Methods Appl. Mech. Eng.* 194, 5191–5220.
- Lussardi, L., Negri, M., 2007. Convergence of nonlocal finite element energies for fracture mechanics. *Numer. Funct. Anal. Optim.* 28, 83–109.
- Marconi, V., Jagla, E., 2005. Diffuse interface approach to brittle fracture. *Phys. Rev. E* 71, 036110.
- Mariani, S., Perego, U., 2003. Extended finite element method for quasi-brittle fracture. *Int. J. Numer. Methods Eng.* 58, 103–126.
- Mazars, J., Pijaudier-Cabot, G., 1996. From damage to fracture mechanics and conversely: a combined approach. *Int. J. Solids Struct.* 33, 3327–3342.
- Meschke, G., Dumstorff, P., 2007. Energy-based modeling of cohesive and cohesionless cracks via X-FEM. *Comput. Methods Appl. Mech. Eng.* 196, 2338–2357.
- Moës, N., Belytschko, T., 2002. Extended finite element method for cohesive crack growth. *Eng. Fract. Mech.* 69, 813–833.
- Moës, N., Dolbow, J., Belytschko, T., 1999. A finite element method for crack growth without remeshing. *Int. J. Numer. Methods Eng.* 46, 131–150.
- Mumford, D., Shah, J., 1989. Optimal approximations by piecewise smooth functions and associated variational problems. *Commun. Pure Appl. Math.* 42, 577–685.
- Naik, R., Prabhakaran, R., 1987. Failure modes for polycarbonate under clearance-fit pin-loading. *Polym. Eng. Sci.* 27 (22), 1681–1687.
- Negri, M., 1999. The anisotropy introduced by the mesh in the finite element approximation of the Mumford–Shah functional. *Numer. Funct. Anal. Optim.* 20, 957–982.
- Oliver, J., Huespe, A., Pulido, M., Chaves, E., 2002. From continuum mechanics to fracture mechanics: the strong discontinuity approach. *Eng. Fract. Mech.* 69, 113–136.
- Ortiz, M., Pandolfi, A., 1999. A class of cohesive finite elements for the simulation of three-dimensional crack propagation. *Int. J. Numer. Methods Eng.* 44, 1267–1282.
- Peerlings, R., de Borst, R., Brekelmans, W., Geers, M., 1998. Gradient-enhanced damage modelling of concrete fracture. *Mech. Cohes.-Frict. Mater.* 3, 323–342.
- Pijaudier-Cabot, G., Bazant, Z., 1987. Nonlocal damage theory. *J. Eng. Mech.* 113, 1512–1533.
- Ramtani, S., Berthaud, Y., Mazars, J., 1992. Orthotropic behavior of concrete with directional aspects: modelling and experiments. *Nucl. Eng. Des.* 133, 97–111.
- Raous, M., Cangèmi, L., Cocu, M., 1999. A consistent model coupling adhesion, friction, and unilateral contact. *Comput. Methods Appl. Mech. Eng.* 177, 383–399.
- Remmers, J., de Borst, R., Needleman, A., 2008. The simulation of dynamic crack propagation using the cohesive segments method. *J. Mech. Phys. Solids* 56, 70–92.
- Song, J.-H., Wang, H., Belytschko, T., 2008. A comparative study on finite element methods for dynamic fracture. *Comput. Mech.* 42, 239–250.
- Xu, X.-P., Needleman, A., 1994. Numerical simulation of fast crack growth in brittle solids. *J. Mech. Phys. Solids* 42 (9), 1397–1434.